REPORT DOCUMENTATION PAGE

Form Approved
OMB No. 0704-0188

1. REPORT DATE *(DD-MM-YYYY)*	2. REPORT TYPE	3. DATES COVERED *(From - To)*
NOV 08	Conference Paper Postprint	Oct 05 – Oct 07

4. TITLE AND SUBTITLE

CHARACTERIZATION OF AN ELECTRO-ABSORPTION MODULATOR DESIGN WITH HIGH-DYNAMIC RANGE FOR BROADBAND ANALOG APPLICATIONS

5a. CONTRACT NUMBER
In-House

5b. GRANT NUMBER

5c. PROGRAM ELEMENT NUMBER
62702F

6. AUTHOR(S)

R. Bussajager, R. Erdmann, R. Michalak, P. Cook, B. McKeon, H. Zmuda, S. Tan, N. Stoffel, C. Schick, T. McDonald, P. Yu, I. Shubin and X. Xie

5d. PROJECT NUMBER
SEMI

5e. TASK NUMBER
SN

5f. WORK UNIT NUMBER
01

7. PERFORMING ORGANIZATION NAME(S) AND ADDRESS(ES)

AFRL/RYDP
525 Brooks Rd.
Rome NY 13441-4505

8. PERFORMING ORGANIZATION REPORT NUMBER

9. SPONSORING/MONITORING AGENCY NAME(S) AND ADDRESS(ES)

AFRL/RYDP
525 Brooks Rd.
Rome NY 13441-4505

10. SPONSOR/MONITOR'S ACRONYM(S)

11. SPONSORING/MONITORING AGENCY REPORT NUMBER
AFRL-RY-RS-TP-2008-8

12. DISTRIBUTION AVAILABILITY STATEMENT

Approved for public release; distribution unlimited. PA# AFRL WS 07-0387

13. SUPPLEMENTARY NOTES

Paper published in Proc. of SPIE Vol 6975, 69750N. This material is declared a work of the U. S. Government and is not subject to copyright protection in the United States.

14. ABSTRACT

An electro-absorption modulator (EAM) is designed to optimize dynamic range performance over 20 GHz bandwidth. The single stripe waveguide enables an extremely compact and integrated package to be fabricated with single mode fiber pigtails. The transfer function's shape permits suppression of higher order intermodulation products, yielding a spur-free dynamic range exceeding that of Mach-Zehnder designs. A dilute optical core diverts energy flow from absorbing layers into a low loss waveguide; the 20 dBm optical power tolerance is significantly higher than that o commercially available electro-absorption devices. The tunable performance over 20GHz is characterized and applications are discussed. New approaches to the broadband impedance matching requirements are calculated and the impact on system performance is assessed.

15. SUBJECT TERMS

Electro-absorption modulator (EAM), fiber technology, spur-free dynamic range

16. SECURITY CLASSIFICATION OF:			17. LIMITATION OF ABSTRACT	18. NUMBER OF PAGES	19a. NAME OF RESPONSIBLE PERSON
a. REPORT	b. ABSTRACT	c. THIS PAGE			Richard Michalak
U	U	U	UU	15	19b. TELEPHONE NUMBER (*Include area code*) N/A

Characterization of an electroabsorption modulator design with high-dynamic range for broadband analog applications

Rebecca Bussjager, Air Force Research Laboratory, RIEA
Reinhard Erdmann, Richard Michalak, Air Force Research Laboratory, RITC
Paul Cook, Air Force Research Laboratory, RITB
Brian McKeon, Air Force Research Laboratory, RYDP
Henry Zmuda, University of Florida, Gainesville
Songsheng Tan, Nancy Stoffel, Charles Schick, Terrance McDonald
Infotonics Technology Center
Paul Yu, Ivan Shubin, Xiaobo Xie, University of California, San Diego

ABSTRACT

An electroabsorption modulator (EAM) is designed to optimize dynamic range performance over 20 GHz bandwidth. The single stripe waveguide enables an extremely compact and integrated package to be fabricated with single mode fiber pigtails. The transfer function's shape permits suppression of higher order intermodulation products, yielding a spur-free dynamic range exceeding that of Mach-Zehnder designs. A dilute optical core diverts energy flow from absorbing layers into a low loss waveguide; the 20 dBm optical power tolerance is significantly higher than that of commercially available electroabsorption devices. The tunable performance over 20 GHz is characterized and applications are discussed. New approaches to the broadband impedance matching requirements are calculated and the impact on system performance is assessed.

Keywords: electroabsorption modulator, EAM, fiber technology, spur-free dynamic range

1.0 INTRODUCTION: APPLICATIONS OF EAM TECHNOLOGY

Many analog applications such as RADAR require high dynamic range; some of those operate at high bandwidth (BW) (~100 MHz), while still others entail frequency agility over wide ranges to 20 GHz. Electro-optic based systems offer significant size and weight reduction, both of which are critical in air platforms, as well as enhanced immunity from electromagnetic disturbance. Despite technical advances in the field, a remaining obstacle to implementation has been the nonlinear distortion inherent in traditional sinusoidal Mach-Zehnder (MZ) based response functions, which define the limit to the spur-free dynamic range (SFDR). Even in a narrow (single octave) bandwidth, the third order intermodulation (IM3) products, such as 2f1 - f2, are so close to the signal frequency that effective filtering is precluded. The response function for a MZ limits this SFDR to about 100 $dB/Hz^{2/3}$ at reasonable laser power (10 - 50 mW), without additional system complexity which is introduced with coherent detection, balanced receivers, or interferometric compensation. An EAM on the other hand is simpler, more compact and involves no interferometric effect. Furthermore, all of our testing was performed with straightforward direct detection, and therefore, constitutes a lower limit to further optimized performance. The form of the EAM's transfer function is not sinusoidal and has been shown to enable effective suppression of the limiting third order distortion products, so as to limit system performance by the lower value of the 5^{th} order distortion [1].

The SFDR performance for the EAM prototype, tested with only 1 mW of laser input power, exceeded 100 $db/Hz^{4/5}$ and increased with higher laser power. We also measured a commercial EAM device manufactured by CyOptics; it was fully packaged was produced and tailored for digital telecom applications. This type of product paves the road to further promoting the viability of EAMs in packaged devices optimized for analog application.

Enabling Photonics Technologies for Defense, Security, and Aerospace Applications IV,
edited by Michael J. Hayduk, Peter J. Delfyett, Jr., Andrew R. Pirich, Eric J. Donkor,
Proc. of SPIE Vol. 6975, 69750N, (2008) · 0277-786X/08/$18 · doi: 10.1117/12.784225

2.0 EAM DEVELOPMENT

Prototype EAM modulators were developed, fabricated, and tested. The designs by Paul Yu at UCSD focused on maximizing the SFDR performance in an analog application. The wafers were processed at CyOptics and integrated in a specially designed fiber pigtailed package at Infotonics Technology Center. Performance testing was done at AFRL, Rome, NY and also at UCSD. CyOptics also provided a commercial integrated EAM in current production for digital telecom applications.

Electroabsorption modulators have been shown to exceed the dynamic range of other optical approaches such as waveguide integrated Mach Zehnder modulators [2]. This has been achieved by Paul Yu at UCSD using several designs on probed waveguides in a laboratory setting. It was well known that transmission and matching of electrical signals, as well as optical fiber to waveguide interfacing, posed significant challenges to realizing the performance of a waveguide chip in a laboratory. The latter's impressive dynamic range results, with useful gain over a large span of frequencies beyond 20 GHz, were influential in motivating this work [2,3]. To take this to another stage in the process necessary to qualify such technology for higher levels of system readiness, an essential step is a sealed packaged product shown in Figure 1 and is suitable for insertion in various brass-board test configurations. Ultimately, it must qualify its operation in various non-laboratory environments. The process of enabling the packaging effort and measuring some of the progress in performance that resulted is the primary focus of this paper. The work is not complete and further progress is expected. A description of the packaging development and device details is given in the following paper #6975-24 by Stoffel, et al. This paper primarily discusses measurement and specification of dynamic range.

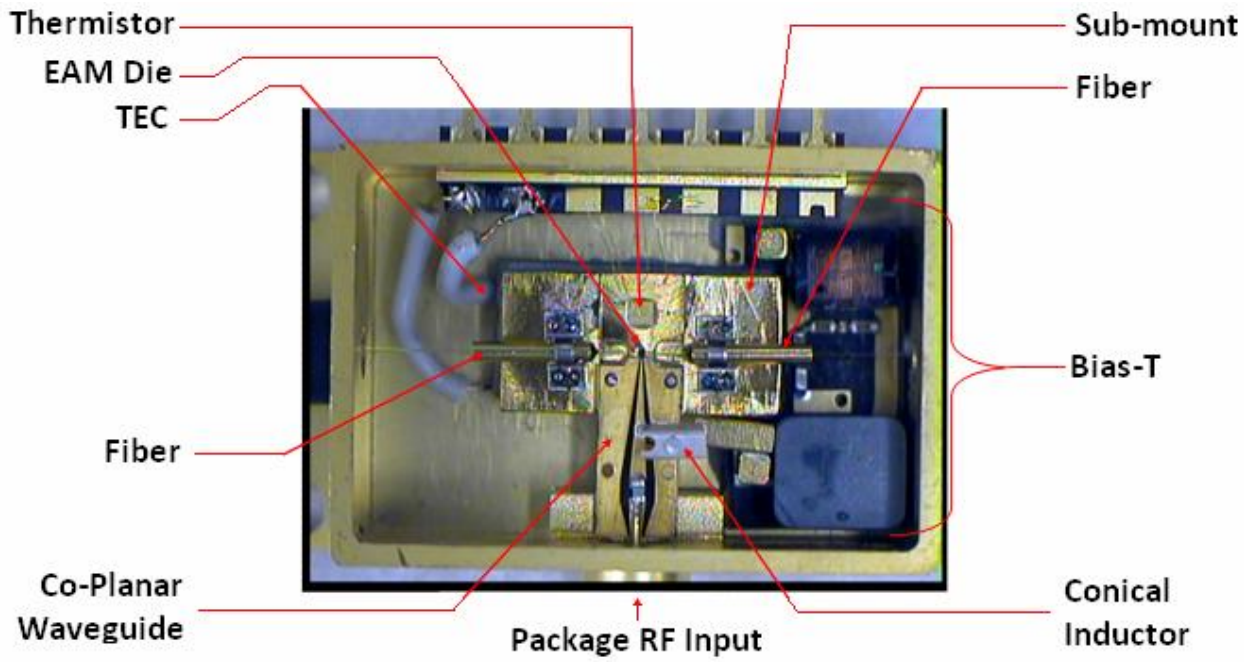

Figure 1. The photo shows the EAM package in a standard 7-pin butterfly mount, RF connector port, and fiber pigtails for optical input and output. EAM design was from Paul Yu at UCSD, wafer processing was performed at CyOptics, and package design and assembly were done at Infotonics Technology Ctr.

The waveguide design made use of the Franz-Keldysh effect. The Dilute Optical Core (DOC) design accomplished a dual purpose of circularizing the optical mode and reducing the optical flux density allowing higher power, hence enhanced SFDR limits. Figure 2a and 2b illustrate a traditional mode field compared to an enhanced mode field shape using a DOC design.

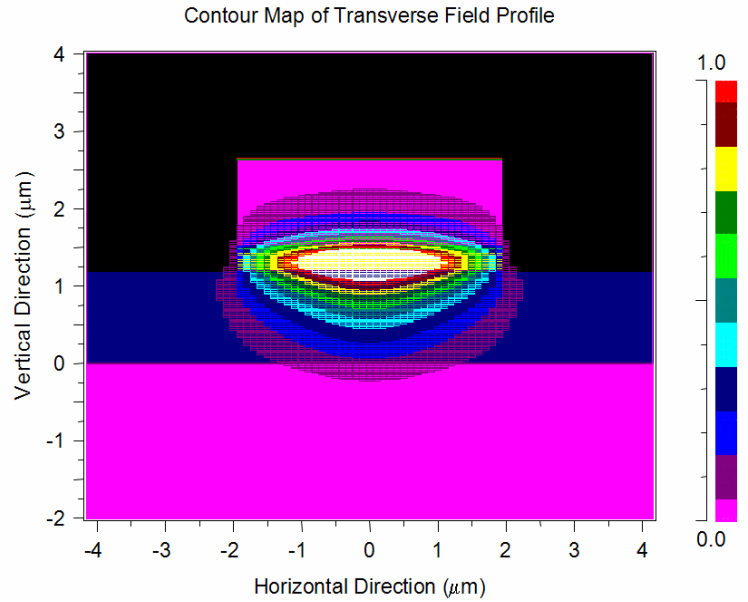

Figure 2a. EAM mode field shape in waveguide is typically asymmetric, reducing the fiber coupling efficiency.

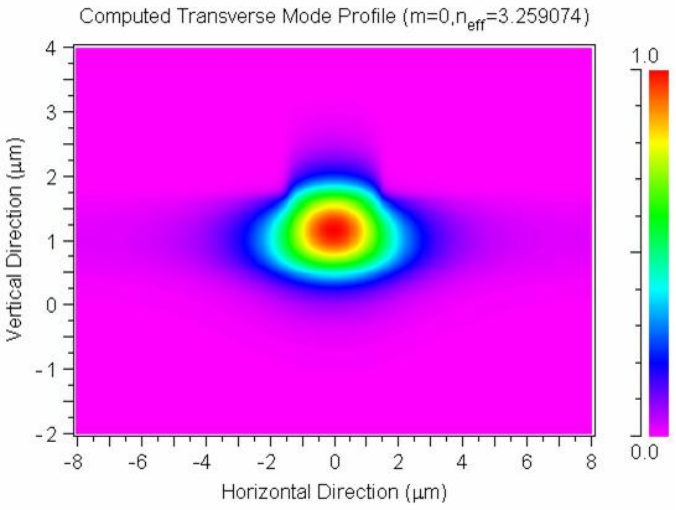

Figure 2b. Highly Symmetric Mode field results from a Dilute Core Design, wherein most of the optical power is transmitted in a non-active waveguide layer.

The transfer function for the unmatched prototype (plotted squares) is shown in Figure 3 at 1 mW optical power a maximum gain (highest slope) at approximately -1.5 V applied bias. The absorption, increasing with higher (negative) voltage, is non-sinusoidal, and can be approximated by use of higher order polynomials for calculating nonlinear effects [1].

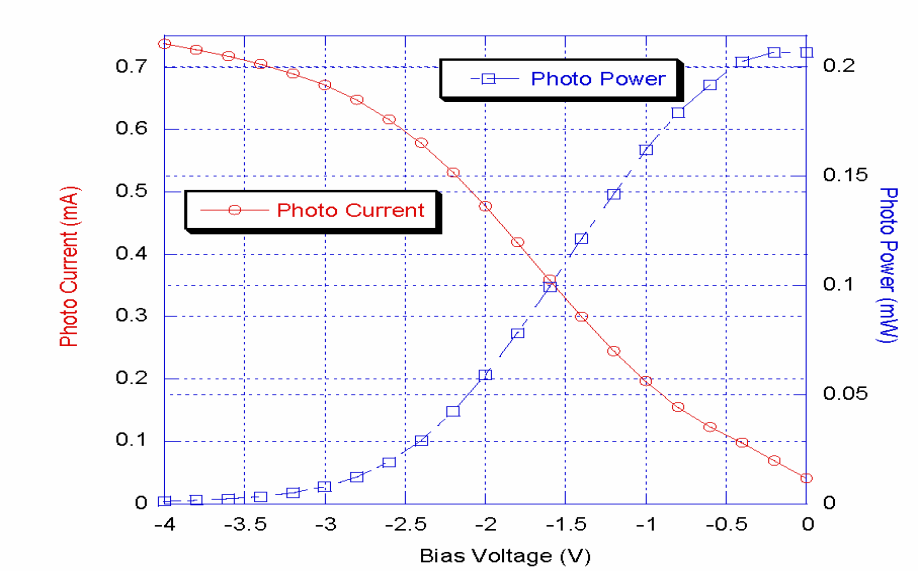

Figure 3. EAM Prototype photocurrent and power vs. bias voltage at input optical power of 1 mW @ 1550 nm.

3.0 EXPERIMENTAL RESULTS

RF reflection loss, S_{11}, and electro optic modulation output, S_{21}, are shown in Figures 4a and 4b for frequencies from 0 to 20 GHz for the unmatched and the matched prototypes, respectively. These were measured on a system with a calibrated optical detector and RF source.

The unmatched EAM prototype's throughput is given in the S_{21} curve in Figure 4a. As expected the S_{11} curve shows considerable reflection in this device except for the anomalous region between 9.5 and 10 GHz.

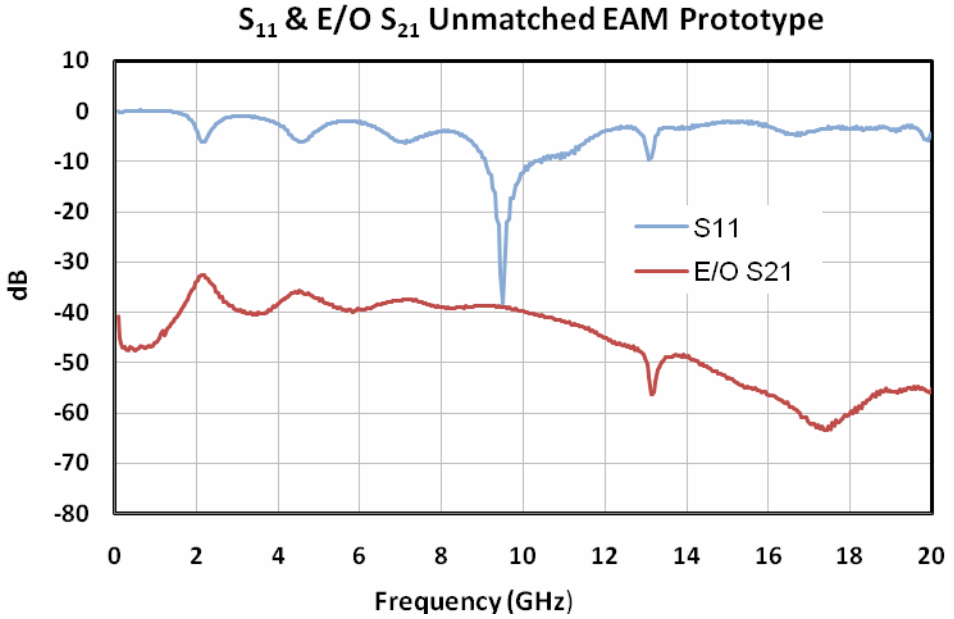

Figure 4a. Microwave spectral response of Unmatched EAM Prototype. Applied laser power is 10.6 mW. Voltage bias on the EAM was adjusted to -1.360 V which gave the highest SFDR. The optical power out of the EAM was 1.98 mW.

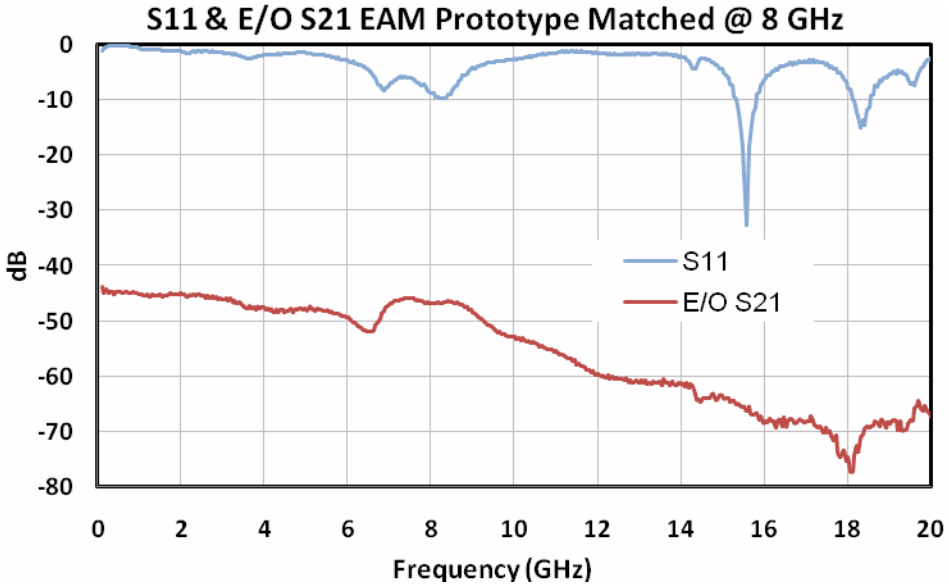

Figure 4b. Microwave spectral response of EAM prototype matched @ 8GHz. Applied laser power was 3.04 mW and optical power out of the EAM was 0.520 mW. Voltage bias on the EAM was adjusted to -0.850 V, which gave the highest SFDR.

In Figure 4b the matched EAM device shows improvement in both the S_{21} and the S_{11} response curves compared to the unmatched EAM device, particularly near the 8 GHz region, where the S_{11} reflection curve shows a significant improvement in reflected power. The S_{21} response in this frequency range displayed the expected peak from the microwave design, but its overall response was lower due to the effect of the different bias setting used for each device. It is important to remember that the EAM is modulated by the applied electric field and does not depend on the power delivered to the device or its matching network. System considerations often dictate that the amplifier driving the EAM not have to handle large reflected signals returning from the EAM as this causes increased power dissipation in the amplifier. This is the primary reason for reducing reflected power (S_{11}).

The CyOptics and two prototype EAMs had SFDR measurements performed at a nominal frequency of 1 GHz. Table 1 shows the link gain of each of the devices as -34.7, -33.2, and -48.6 dB. These were arrived at by careful measurement at the 1 GHz test frequency and are accurate with the understanding that the measurements include the optical detector responsivity and RF gain at 1 GHz. The corresponding S_{21} measurements taken from the graphs are at significantly different from the link gain measurements because the link gain measurements were taken at different optical powers, different voltage biases, and used different detectors, whereas the S_{21} data were all taken with the same equipment, although bias and optical power differed. The S_{21} data is presented to show the relative spectral responses of the EAMs.

Table 1. Key Data Summary

EAM	SFDR	Link Gain (dB)	Bias Voltage	Noise Floor dBm/Hz	Laser Power In (mW)	Laser P Out (mW)	Test f (GHz)	IM3 f (GHz)	Conditions
CyOptics E4560D	108.7 $dB/Hz^{4/5}$	-34.7	-0.796	-164.6	20 mW (Estimated)	3.5	1.000 0.975	1.025	
EAM-Unmatched	114 $dB/Hz^{4/5}$	-33.2	-1.430	-162.9	10.6	1.82	1.000 1.025	0.975	No Thermal Control
EAM-Matched	102 $dB/Hz^{4/5}$	-48.6	-1.170	-162.6	25.6	3.60	1.000 1.025	0.975	

3.1 Theoretical model: SFDR dependence [1]

Equation 1 mathematically depicts the SFDR:

$$SFDR = \frac{\langle P_{IM3}(m_{sf})\rangle^2}{\frac{2kT}{\langle I_d\rangle^2}R_{out} + \frac{4e}{\langle I_d\rangle} + \frac{8kTR_{in}^2}{V_{\mathrm{mod}}^2} + \frac{16e\langle I_m\rangle R_{in}^2}{V_{\mathrm{mod}}^2} + 2r^2}, \quad (1)$$

where I_m is the modulator current; $R_{in,}$ R_{out} are input and output resistances; kT is the Boltzman thermal energy; r is the laser RIN noise; V_{mod} is the equivalent V_π bias; e is the electronic charge; $P_{IM3}(m_{sf})$ is the 3rd order intermod spurious power level at the noise floor; I_d is the detector photocurrent and proportional to the optical input power; with limits when:

$<I_d> <<1$; kT thermal noise dominates

$<I_d> \sim 1$; shot noise dominates by e

$<I_d> >>1$; $<I_m>R_{in}^2$ amplified noise input or r RIN noise dominates.

The input power levels measured in this report were all in the intermediate range, where the shot noise term dominates and implies a linear increase in SFDR with optical input power, $<I_d>$. At the very high power levels, not reached here, this linear increase in SFDR breaks down as the noise power grows with the signal.

3.2 SFDR measurements

The test setup for intermodulation distortion measurements, shown in Figure 5, was used to determine the SFDR of the EAMs. The CyOptics commercial device tested had its own integral laser while the EAM prototypes used an external 1558 nm laser. The bias supply drift and noise were less than 10 microvolts. Link gain measurements were taken by subtracting the measured RF level at the EAM input from the measured RF level from the light detector. The low noise amplifier puts the signal noise originating from the EAM above the noise of the spectrum analyzer. Because of differing RF reflection losses between the two tones from the EAM RF port, leveling at the EAM RF port would not have delivered equal modulation power to the EAM. Since the objective of the test was to measure distortion resulting from modulation, the two tones were leveled by measuring RF modulated light output from the detector. Figure 6-8 show measured SFDR results on the CyOptics device and the effect of bias variation.

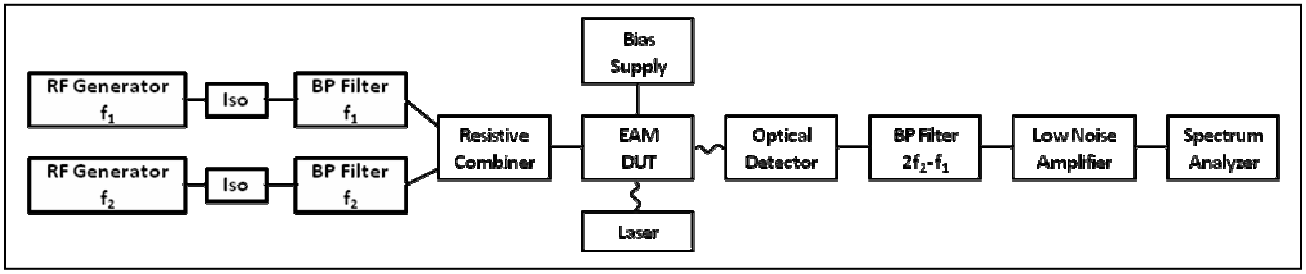

Figure 5. Test setup for SFDR Measurements.

In Figure 6, at an optimum bias voltage tuned to a null of the EAM's third harmonic response, the IM3 response (heavy black trace) exhibits a linear slope of 5 throughout the range of RF power to the noise floor. At nearby bias values, transition zones from slope 3 to slope 5 are manifested in the IM3 response traces. Note that at output RF powers > 105 dB, all slopes converge. This implies that for 165-105 = 60 dB elevation above the noise floor, all bandwidths > 10^6 Hz will have SFDR values determined entirely by the slope 5 trace. Since bandwidths in practical systems are nearly all one MHz or greater, this implies that the bias voltage tuning in the EAM is not necessarily ultra critical in actual practice.

In Figure 7, the slope 5 SFDR (dark black line) of 108.7 dB/Hz$^{4/5}$ in normalized scaled units indicates that at -0.778 V bias at 10 KHz BW (40 dB above NF)the SFDR is given by 108.7 – 4/5(40) = 76.7 dB. Note, however, that by tuning the

bias to -0.796 V the SFDR can be increased *at that BW* to approximately 84 dB. This feature of EAMs permits SFDR in certain BW regions to be optimized, as shown by the variation of transition zones with bias in the prior figure.

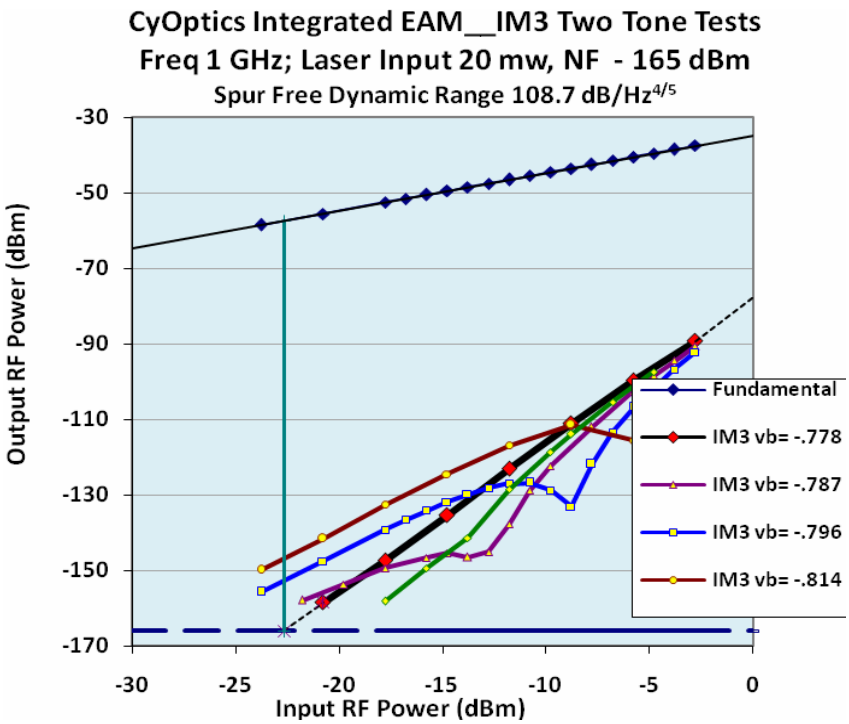

Figure 6. CyOptics device tested illustrating effect on the SFDR by varying the applied bias. Results for IM3 testing at 1 GHz with 20 mW input power.

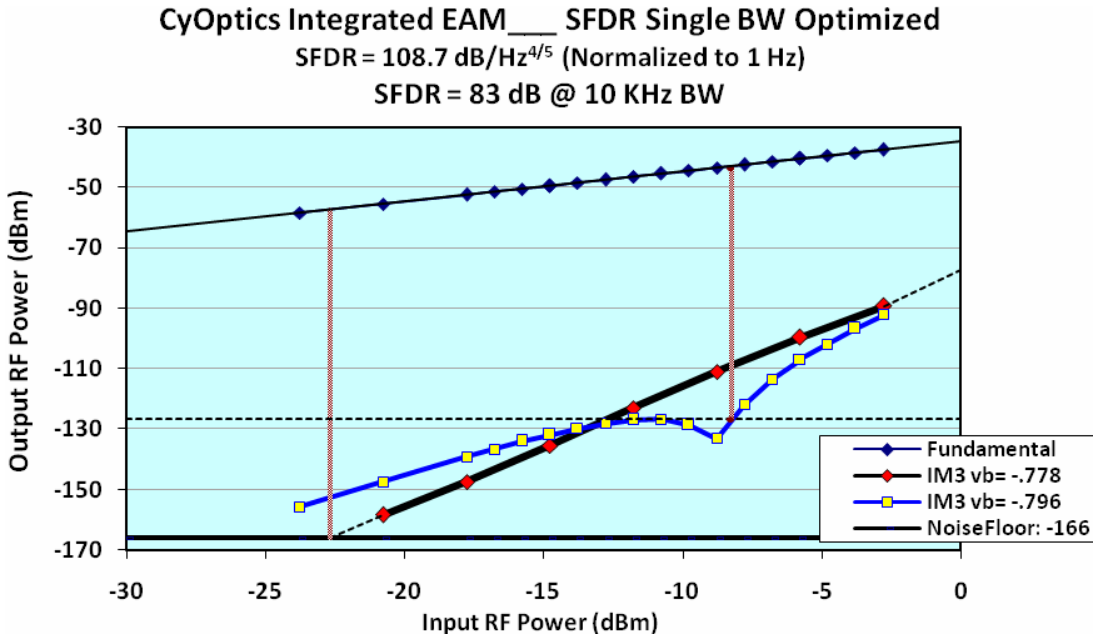

Figure 7. CyOptics device tested illustrating effect on the SFDR by varying the applied bias. Results for IM3 testing at 10 KHz with 20 mW input power.

The plot in Figure 8 illustrates the variation of SFDR *at 1 Hz bandwidth* with bias voltage on the CyOptics device. Note that each value is based on the intersection at the 1 Hz noise floor, but because the slopes are not single valued in this case, the units cannot be scaled to project SFDR values at other BWs.

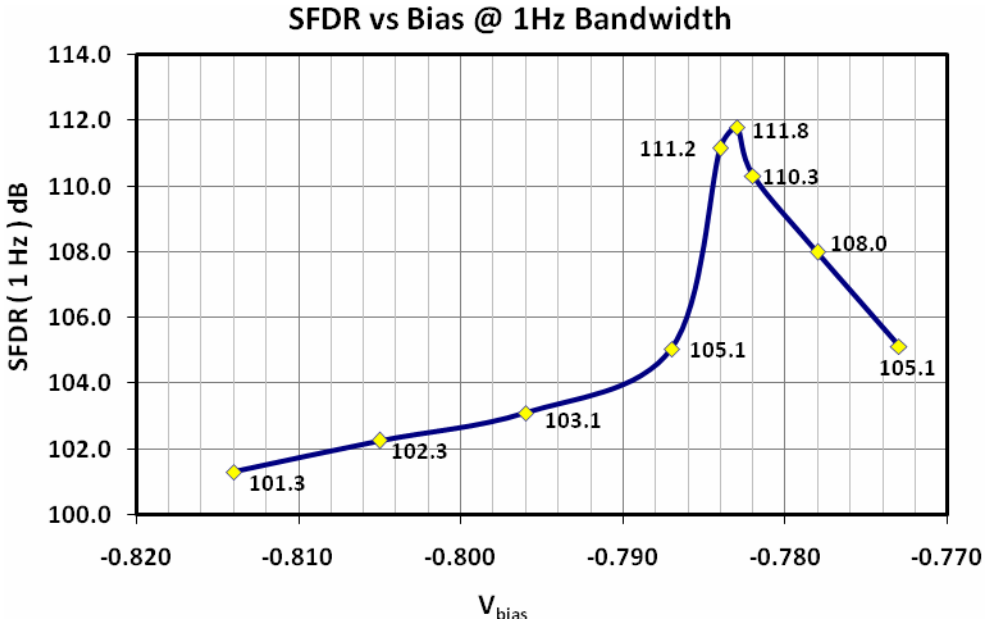

Figure 8. CyOptics device tested illustrating effect on the SFDR *at 1 Hz bandwidth* with varying the applied bias.

The SFDR data shown in Figure 9 show both upper and lower odd order side bands. These measurements were made by swapping out the $2f_2$-f_1 bandpass filter located after the optical detector (Figure 5). The two curves are essentially identical and in good agreement with theory. Figures 7, 9, and 10 show SFDR data from only one side band as a set of only three matched filters were available for these measurements. These three filters can be rearranged by swapping a primary tone filter with the sideband filter to give an approximation of upper and lower sideband measurements but are not precisely the same as exact measurements taken with a set of four matched filters. That is, because the measurements taken with only three filters do not use the same primary tones, the two measurements will not necessarily match. Despite this the three filters used for taking the data in Figures 7, 9, and 10 were swapped to check "the other sideband". For instance the CyOptics device in Figure 7 was tested with 1.000 and 0.975 GHz primaries, and the IM3 was measured at 1.025 GHz -- but primaries of 1.000 GHz and 1.025 GHz and an IM3 filter of 0.975 GHz could have been used by rearranging the filters, as they were for the unmatched EAM device shown in Figure 11. The filter arrangements used were chosen to give the best SFDR results. In some cases the alternate filter arrangement gave significantly poorer results, and it should be noted that one would not expect this from theory.

The data shown in Figures 9 and 10 were measured on the same device design at different input power levels; those support the predicted linear increase, i.e. a 10 dB increase in optical power resulted in about 9 dB increase in the measured SFDR. This shows that input power is itself a critical parameter, and also the importance of the use of a dilute optical core design permitting higher power levels in the EAM.

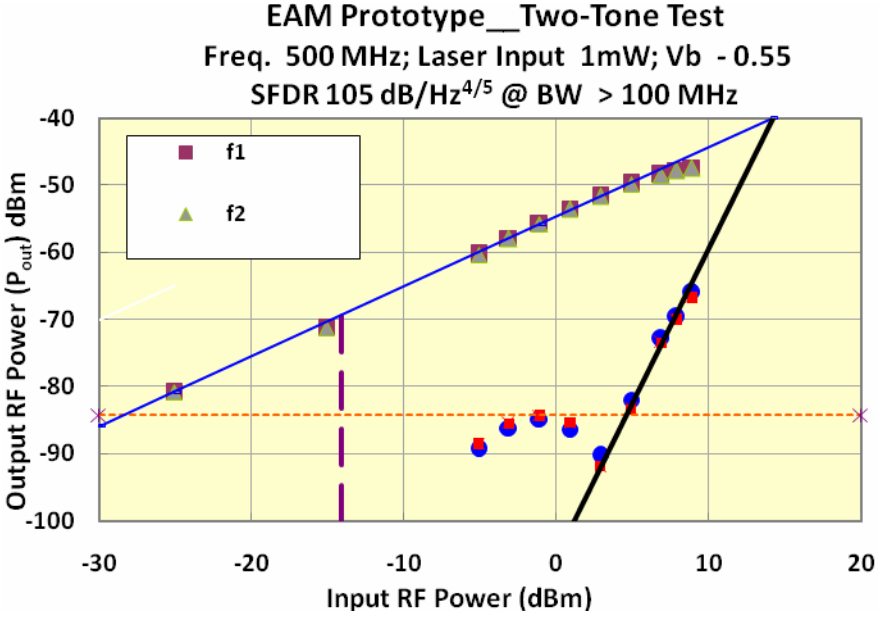

Figure 9. The SFDR value of 105 dB/Hz$^{4/5}$ based on the noise floor intercept was achieved in this EAM with the remarkably low optical input power of only 1 mW. It applies strictly to the slope 5 portion of the trace above the dotted line, indicating a bandwidth cutoff of ~ 100 MHz based on the elevation above the Noise Floor. [Data in this plot was taken at USCD on an Unmatched Prototype].

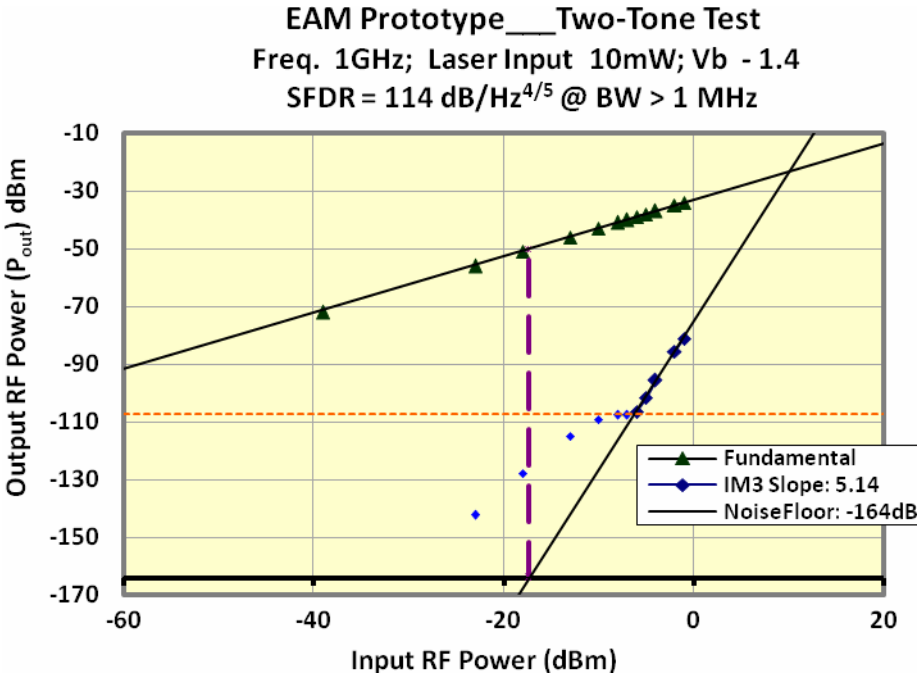

Figure 10. Device design was identical to that in Figure 9. At 10 mW input power, an expected increase in SFDR to 114 dB/Hz$^{4/5}$ was observed in testing at AFRL. The SFDR based on NF intercept applies here to all BWs > 1 MHz (above dotted line at 105 dBm, 60 dB above NF). This would include nearly all systems of practical interest, for which the transition to slope 3 at lower BWs can be neglected.

3.3 Measurement analysis

SFDR tests showed that the EAM prototype matched at 8 GHz tested at 1 GHz, gave lower gain and SFDR than the other devices. (Test filters at 8 GHz were not available at the time.) The prototype unmatched tested at 500 MHz with 1 mW yielded high performance and served as a reference to confirm the SFDR power scaling. The CyOptics with ~20 mW fixed input power, (at frequency 1 GHz) also yielded a high SFDR performance in these analog tests, considering that it was designed for digital application. The highest SFDR was measured on the unmatched EAM Prototype at only 10 mW input power (also at 1 GHz). This DOC design permits significantly higher input power, and the tests now in process project a SFDR > 120 dB/Hz$^{4/5}$ at ~50 mW input power. All tests reported here were for single octave bandwidth, which meets the requirements of many practical systems (e.g.100 MHz BW @ 8 GHz carrier; SFDR = 120 – (4/5)80 = 56 dB). The same bias control methods for EAMs can also be applied to broadband application by suppression of IM2 rather than IM3, though that was not pursued in these tests. Tests were also performed at 10 GHz to confirm the theoretical expectation that SFDR is not strongly dependent on frequency.

Figure 11 shows calculated nonlinear effects using MathCAD software. The darkened black line is at optimum bias for slope 5 throughout, with scaled SFDR of 120 dB/Hz$^{4/5}$. The dashed trace shows SFDR of 124 dB *@ 1 Hz BW only*, an increase of 4 dB. The blue (next higher) trace also shows 4 dB increase over the SFDR given by slope 5 projection at 100 KHz BW, and the pink (next) trace yields a similar increase at 100 MHz. Evidently by tuning the bias to optimize a *single* BW the "effective SFDR" can be increased by approximately 4 dB at every BW. Note that this effect is distinct from the global SFDR bias setting for 120 dB/Hz $^{4/5}$at slope 5, which is completely independent of BW! The other plots show that for any *singly optimized* BW, SFDR reverts to that given by slope 5 for higher BWs, and reverts to that given by slope 3 for all lower BWs.

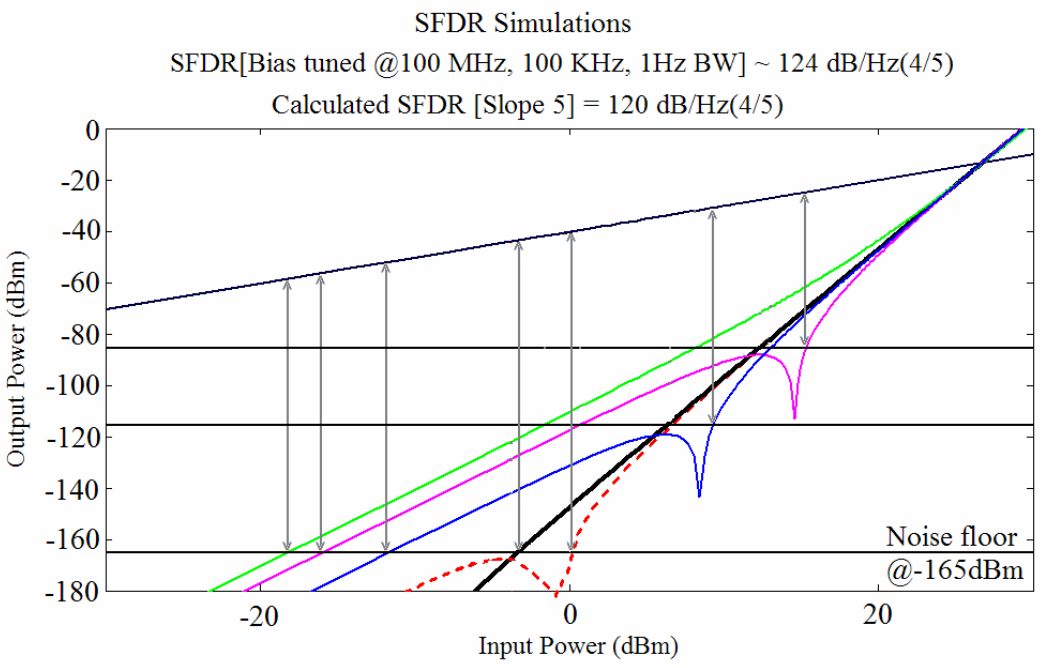

Figure 11. Calculated nonlinear effects using MathCAD software. The darkened black line is at optimum bias for slope 5 throughout, with scaled SFDR of 120 dB/Hz$^{4/5}$.

3.4 Generalized specification of SFDR for EAMs

Because EAMs offer the distinctive feature of exhibiting multiple slopes for IM3 response *within practical power* ranges, this feature also permits SFDR to be optimized at single BWs. However, unambiguous specification of SFDR

becomes more challenging, in particular if we are to retain the convenience of a "single valued" SFDR performance characterization, rather to specify it separately at every BW. Figure 11 serves to both illustrate and suggest a distinct notation for single bandwidth SFDR specification. In the calculated example given there, the s*ingle badnwidth SFDR = 124 dB/Hz* $^{4/5}$ designates this as being single bandwidth optimized, where the bias must be tuned for each bandwidth to be optimized. The usual notation convention [4] **SFDR = 120 dB/Hz** $^{4/5}$ applies to the bias setting which exhibits a single slope of 5 applicable to all bandwidths, without bias tuning. This is in complete analogy with other standard components and MZs, except that the IM3slope value can be 5 rather than the typical value of 3. Whether the option of single bandwidth SFDR optimization is advantageous depends on whether the system operates near a single bandwidth. If it must cover a wide range of bandwidths, then the broadband single slope setting is appropriate. Such choice of operation methodology is not available in other technical approaches, such as conventional MZs, and can make EAMs more flexible in various systems.

In all of the key results given in Figures 6-10, all SFDR values were determined by direct measurement, with the relevant BW cutoff clearly designated for each case by established convention. The difference between the SFDR at 1 Hz BW and the SFDR scaled units of dB/Hz$^{4/5}$ was also clarified. The latter gives SFDR at all other BWs of interest in accord with the notation designed for that purpose. The SFDR at 1 Hz only is not of interest in itself since systems do not operate at that BW. The calculated simulations, Figure 11 though very useful, were not used to establish the actual SFDR values, those were measured, rather calculation was to illustrate parameter variation, and how those affect a generalized EAM specification method proposed here.

4.0 CONCLUSION

EAM devices have demonstrated high SFDR and high power tolerance in probed laboratory settings; this packaged version makes those suitable for interchange and cross-prototype testing. The cooperative effort on the part of AFRL, UCSD, Infotonics Technology Ctr., CyOptics Inc. resulted in a fully packaged electroabsorption modulator, suitable for performance and reliability tests. Such devices offer very significant size and weight reduction in analog aircraft and remotely accessed ground based antennas. A key limiting performance parameter, SFDR, was directly measured on several packaged prototypes, and found to satisfy preliminary benchmarks for existing RADAR and other applications. The performance in a single octave of bandwidth exceeds that of other electro-optic approaches at comparable input power, and its instantaneous bandwidth can be rapidly tuned over a 20 GHz frequency range in a properly matched receiver system. The projection to greater than 120 dB/Hz$^{4/5}$ at moderate optical power is conservatively based on direct detection without optimum microwave matching, therefore permits further improvement. Enhanced performance with higher incident powers remains under active development at UCSD.

Acknowledgements: Appreciation to Michael Fanto (AFRL-RITC) for essential technical support and fiber coupling of EAM devices.

REFERENCES

1. Robert B. Welstand, "High linearity Modulation and Detection in Semiconductor Electroabsorption Waveguides," *PhD Dissertation, University of California*, Electrical Engineering, San Diego, 1997.

2. Y.Zhuang, W.Chang, P. K. L. Yu, "Peripheral-Coupled-Waveguide MQW Electroabsorption Modulator for Near transparency and High Spurious Free Dynamic Range RF Fiber-Optic Link", *IEEE Photonics Technology Letters*, Vol. 16, No. 9, pp. 2033-2035, 2004.

3. J. Önnegren, J. Svedin, O. Sahlén, M. Jansson, A. Alping, "Analog characterization of a Franz-Keldysh electroabsorption modulator monolithically integrated with a DFB laser," *Optical Technology for Microwave Applications VII*, *Proc. SPIE,* Vol. 2560, pp. 19-30, 1995.

4. J. H. Schaffner, W. B. Bridges, "Intermodulation distortion in high dynamic range microwave fiber-optic links with linearized modulators," *J. Lightwave Technol*., Vol. 11, No. 1, pp. 3-6, 1993.

5. B. S. Yarman and H. J. Carlin, "A Simplified 'Real Frequency' Technique Applied to Broad-Band Multistage Microwave Amplifiers," *IEEE Transaction on Microwave Theory and Techniques*, Vol. MTT-30, No. 12, December 1982, pp. 2216-2222.

6. V. Belevitch, Classical Network Theory , San Francisco, Holden Day, 1968, p. 278.

7. R. M. Fano, "Theoretical Limits on the Broad-Band Matching of Arbitrary Impedance Functions," *Journal of the Franklin Institute*, Vol. 249, No. 1, January 1950, pp. 57-83.

6.0 Appendix: Broadband Matching Considerations

Because the package itself with electrical connections and transmission lines significantly affects the key performance parameters, those must be tested. The results of electrical matching, and mismatching were very evident. The correct solution is a broadband matched design to cover the span 2 to 20 GHz. Such are not available in practice, so a portion of the work was dedicated to investigating designs for implementation in follow on work.
As with any microwave device, parasitic effects such as junction capacitance, bond wire inductance, packaging effects and the like can seriously alter or even degrade the frequency response performance of the device. These effects are especially pronounced for extremely broadband devices such as the EAM device presented resulting in a non-uniform frequency response. A large body of literature exists that addresses the issue of broadband matching. Of the many approaches that exist, the analytical optimization method proposed by Yarman and Carlin [5] is particularly attractive for broadband matching EAM devices.

The general situation is illustrated in Figure A1. A load impedance Z_L represents the EAM and can be specified either analytically or from a model. The ability to proceed directly from measured data is particularly useful when matching to a load that could contain a certain degree of nonlinearity. Although in a laboratory environment the RF/microwave drive signal would most likely be obtained from a 50-ohm lab-quality source, a real application would likely drive the EAM with another microwave device (such as an antenna) whose impedance is not likely to be an ideal 50-ohm termination. Once again, the generator's internal impedance can be specified from a model or directly from measured data.

For a load and generator reflection factor of $S_L = \frac{Z_L - Z_o}{Z_L + Z_o}$ and $S_G = \frac{Z_G - Z_o}{Z_G + Z_o}$, respectively, where Z_o is a constant that is generally chosen to equal the impedance level of the system, the power gain $G_P(\omega)$ of the overall system, defined here as the average power delivered to Z_L divided by maximum power from the generator can be expressed as

$$G_P(\omega) = \frac{|s_{21}(\omega)|^2 \left(1 - |S_G(\omega)|^2\right)\left(1 - |S_L(\omega)|^2\right)}{|1 - s_{11}(\omega)|^2 \left|1 - \left(s_{22}(\omega) + \frac{s_{21}^{\,2}(\omega) S_G(\omega)}{1 - s_{11}(\omega) S_G(\omega)}\right) S_L(\omega)\right|^2} \qquad (1)$$

where $s_{i,j}(s), i, j = 1,2$ are the elements of the two-port scattering matrix of the lossless matching network. Because of the assumed lossless nature of the (yet unknown) matching network, a great deal of structure exits for its mathematical representation. Specifically, it can be shown that the most general form for the scattering matrix that admits a commensurate line realization can be expressed as [6]

$$S(\omega)=\frac{1}{g(s)}\begin{bmatrix} h(s) & s^k \\ \pm s^k & \mp h(-s) \end{bmatrix} \tag{2}$$

where s is the usual complex frequency variable with $h(s)$ and $g(s)$ polynomials satisfying $h(s)h(-s)\pm s^{2k}=g(s)g(-s)$. This structure allows for a simple numerical optimization procedure where one iterates on the coefficients of the polynomial $h(s)=h_0+h_1 s+\cdots+h_N s^N$ while evaluating the gain expression of Equation (1) until the desired performance is achieved. Spectral factorization of $g(s)g(-s)$ and choosing the left-hand-plane roots for $g(s)$ ensures that a realizable lossless matching structure will result.

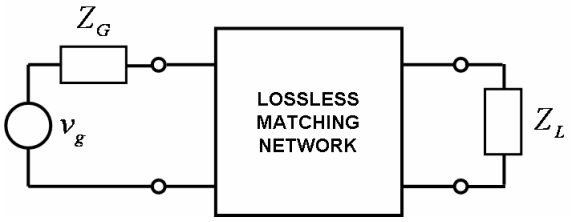

Figure A1. **The general broadband matching problem.**

To illustrate the benefits a simple three-element matching network was designed. Referring to Figure A2, the source impedance consists of an internal resistance along with a coupling capacitor. The load impedance consists of the EAM with the necessary bond wire inductances. The topology of the matching network is a direct result of the synthesis procedure and in this case takes the form of a low-pass ladder. Since the output of the design process yields a rational function of frequency, it may form a lumped element circuit (Figure A2) or a commensurate line network as indicated.

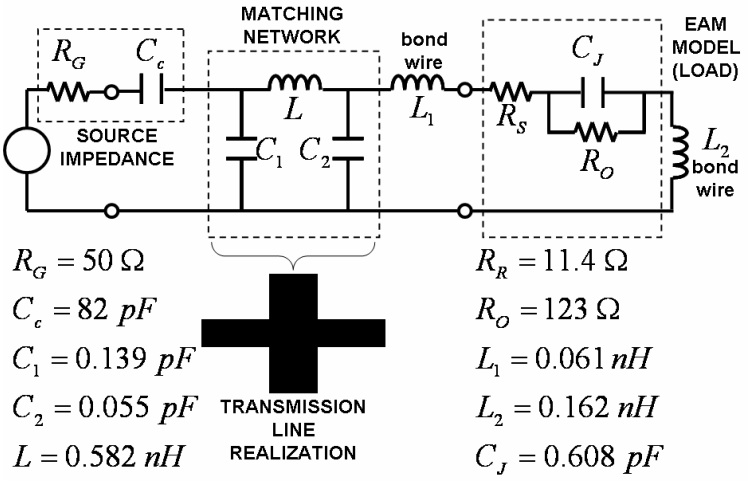

Figure A2. **Three-element matching network example for the EAM.**

Figure A3 shows the simulated overall response obtained from the example given in Figure A2 and indicates the improvement in performance that is expected. It is seen from the figure that even a simple three-element extends the high frequency limit from 5 GHz to roughly 11 GHz as well as providing an overall flat response. Higher order matching networks can be used to further extend the maximum frequency to values approaching the Fano limit [7].

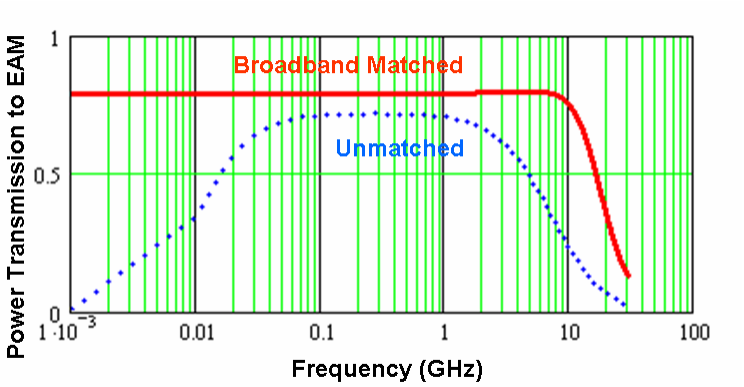

Figure A3. **Comparison of performance for an unmatched EAM with the simulated results of a three-element broadband.**